

Spin Torque Oscillator and Magnetization Switching in Double-Barrier Rashba Zeeman Magnetic Tunnel Junction

Saumen Acharjee*, Arindam Boruah†, Reeta Devi‡ and Nimisha Dutta§
Department of Physics, Dibrugarh University, Dibrugarh 786 004, Assam, India

In this work, we have studied the spin torque based magnetization oscillations and switching in presence of Rashba - Zeeman (RZ), Ruderman - Kittel - Kasuya - Yosida (RKKY) and Dzyaloshinskii - Moriya (DM) interactions in a double-barrier RZ|Heavy Metal (HM)|RZ magnetic tunnel junction (MTJ). The system has stable magnetization oscillations and can work as an oscillator or a switcher for a significant difference in the strength of RKKY and DM interaction under suitable spin transfer torque (STT). For the proposed system with same order of RKKY and DM interaction, a nonlinear characteristic of the magnetization oscillation is observed. However, this nonlinearity of oscillations can be reduced by an external magnetic field or considering a material with suitable RZ interaction. In addition to this, our study reveals the magnetization switching can be tuned by using suitable STT. A dependence of switching time on layer thickness is also observed. Also, the switching speed increases with the thickness for systems having either same order of RKKY and DM interaction or dominated by RKKY interaction. An opposite characteristic is seen when DM interaction dominates over RKKY interaction.

PACS numbers: 72.25.Dc, 72.25.-b, 75.78.-n, 75.75.-c, 85.75.-d

I. INTRODUCTION

Spin torque oscillators (STOs) are nano-sized electronic devices based on magnetic tunnel junctions (MTJ) that have recently received considerable attention due to their wide range of applications [1–12]. STOs are essentially magnetoresistive stacks, where the polarized spin current generates the spin torque [1–3]. Thus, it leads to self-sustaining magnetization oscillations in the free layer. This characteristic of STOs can be utilized to use them as microwave generators, field sensors, phased array antennae etc [4–12]. Another essential phenomenon witnessed in an MTJ is magnetization switching, which is the backbone of current non-volatile magnetic memories [13–17].

Usually, a conventional MTJ consists of a tunnel barrier sandwiched between two ferromagnetic layers, namely, pinned and free layers. However, such arrangements have non-adequate thermal stability below 40 nm [18]. This can be achieved by using double interface MTJs, typically an arrangement of a heavy metal (HM) between two ferromagnetic layers [18–20]. The FM|HM|FM arrangement is vital in enhancing the spin-orbit coupling (SOC) and generating Ruderman - Kittel - Kasuya - Yosida (RKKY) interaction. Due to the presence of RKKY interaction, the magnetizations of the two layers are ferromagnetically coupled [18, 21]. So they can behave like identical layers. Moreover, the strong SOC of HM can also even induce Dzyaloshinskii - Moriya (DM) interaction, which is an antisymmetric exchange coupling, [22, 23]. Recent studies have shown that RKKY interactions may suppress the detrimental effects of DM interactions in STT switching [18]. Thus it is noteworthy to un-

derstand the interplay of SOC, RKKY and DM interaction in STT magnetization dynamics.

Recently discovered Rashba - Zeeman (RZ) effect in Ag_2Te / Cr_2O_3 composite can provide some novel features that are not found in pure Rashba or Zeeman systems [24]. These materials have some unique characteristics and also have the ability to trigger insulator to conductor via an exchange field [24] and can also be used as spin filters [25–27]. In general, the Rashba SOC (RSOC) is an antisymmetric SOC responsible for splitting of energy sub-bands [28–42]. The impact of RSOC on STOs is worth mentioning, which shows the utilization of RSOC in magnetization switching and also its contribution to self-oscillations in STOs. Moreover, the RSOC of the multilayer systems can substantially increase the size of the STO phase [11, 43]. So, it is necessary to understand the role of RSOC and its interplay with RKKY and DMI in STOs and magnetization switching. Though STOs and magnetization switching had been studied in double-barrier MTJs earlier, the introduction of RZ material as a free layer can significantly change auto oscillation and magnetization switching conditions. Moreover, STOs and magnetization switching were not studied in the same frame earlier. Thus in this work, we consider a double-barrier Rashba Zeeman Magnetic Tunneling Junction (RZ-MTJ) where we consider an HM sandwiched between two RZs.

The organization of this paper are as follows: we present a minimal theory to study magnetization dynamics and switching in double interface RZ-MTJ in section II. In Section III, we present the results of our work by considering the effect of RKKY, DMI, RSOC and other important parameters like external magnetic field. We have analysed the effect of the parameter on magnetization dynamics and switching too in this section. Finally, a brief summary of our work is presented in Section IV.

*saumenacharjee@dibru.ac.in

†arindamboruah@dibru.ac.in

‡reetadevi@dibru.ac.in

§nimishadutta@dibru.ac.in

II. MINIMAL THEORY

The schematic representation of a double-barrier RZ based MTJ is shown in Fig. 1. In general a double-barrier MTJ is composed of three magnetic layers viz. reference layer, free/storage layer and control layer. The reference and control layers act as polarisers whose magnetizations can be controlled independently of the free layer [52]. We have considered an FM reference layer and an FM control layer with a RZ|HM|RZ composite free layer for our analysis. A Spin Transfer Torque (STT) is induced in the free layer because of the FM polarisers [18, 52] as shown in Fig. 1. We choose the easy axis anisotropy along the y-direction, while an external magnetic field is considered along the z-direction in our analysis. The time evolution of the magnetization in RZ layers can be studied by using two coupled Landau - Lifshitz - Gilbert - Slonczewski (LLGS) equations.

$$\partial_t \mathbf{m}_j = -\gamma \mathbf{m}_j \times (\mathbf{H}_{\text{eff}} + \mathbf{H}_j^{\text{R}}) + \alpha_j \mathbf{m}_j \times \partial_t \mathbf{m}_j + \mathcal{T}_j^{\text{STT}} \quad (1)$$

where, the indices $j = 1, 2$ corresponds to first and second RZ layers respectively. The parameter γ is the gyromagnetic ratio and α_j is the Gilbert damping parameter of the RZ layers while \mathbf{H}_{eff} is the effective field of the system can be obtained using the effective Hamiltonian \mathcal{H}_{eff} of the system

$$\mathcal{H}_{\text{eff}} = K_{\text{exc}}(\nabla \mathbf{m}_j)^2 - \mathbf{D}_{12} \cdot (\mathbf{m}_1 \times \mathbf{m}_2) + \mathcal{J}_{12}(1 - \mathbf{m}_1 \cdot \mathbf{m}_2) - \mathbf{H}_{\text{ext}}(\hat{z} \cdot \mathbf{m}_j) + h_0 \sigma_j \cdot \hat{m}_j \quad (2)$$

where, K_{exc} incorporate the exchange coupling between the FM and RZ layers, \mathbf{D}_{12} is the DMI vector, $\mathcal{J}_{12} = \frac{\sigma_{\text{exc}}}{\Delta_{12}^2}$ is the ratio of bilinear exchange coefficient between two surfaces with discretion cell dimension [18]. Here, \mathbf{H}_{ext} is the external magnetic field strength and the last term of Eq. (2) gives the contribution of Zeeman energy with h_0 being the strength of Zeeman energy. The Rashba field \mathbf{H}_j^{R} in Eq. (1) is given by [11]

$$\mathbf{H}_j^{\text{R}} = -\frac{1}{1 + \beta^2} \frac{\alpha_R m_e \mathcal{P}_j j_0}{e M_0 \hbar \mu_0} (\hat{y} \times \hat{z}) \quad (3)$$

where, α_R is the RSOC strength with \mathcal{P}_j being the polarization of the current j_0 through the RZ-layers. M_0 is the saturation magnetization and β is the adiabatic damping parameter. It is to be noted that the anisotropy of the system can be incorporated by considering an easy-axis anisotropy field $\mathbf{H}_{\text{an}} = \frac{1}{2} \frac{K_{\text{an}} m_y}{M_0} \hat{y}$ in Eq. (1) [6].

The last term of Eq. (1) corresponds to the spin-transfer torques $\mathcal{T}_j^{\text{STT}}$ acting on the magnetization \mathbf{m}_j and can be given by [11]

$$\mathcal{T}_1^{\text{STT}} = -\tau_1 [\mathbf{m}_1 \times (\mathcal{P}_0 \mathbf{m} - \mathcal{P}_1 \mathbf{m}_2) \times \mathbf{m}_1] \quad (4)$$

$$\mathcal{T}_2^{\text{STT}} = -\tau_2 \mathcal{P}_1 (\mathbf{m}_2 \times \mathbf{m}_1 \times \mathbf{m}_2) \quad (5)$$

where, $\tau_i = \frac{\gamma \hbar j_1}{2e M_0 \mu_0 t_i}$ with the index $i = 1, 2$ corresponds to first and second RZ layers respectively and measured in Jm^5/A^4s . Here, t_i are the thickness while $\mathcal{P}_0, \mathcal{P}_1$ are the

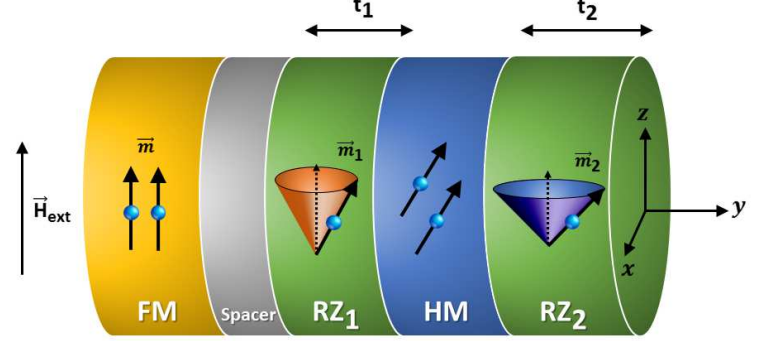


FIG. 1: Schematic illustration of the proposed double-barrier MTJ consisting of Rashba-Zeeman (RZ)|Heavy metal (HM)|Rashba-Zeeman (RZ) hybrid as a composite free layer sandwiched between Ferromagnetic (FM) reference and control layers. The reference and control layers act as polarisers whose magnetizations can be controlled independently of the free layer. As a result an STT is induced in the RZ|HM|RZ composite free layer. \mathbf{m}_1 and \mathbf{m}_2 represent the magnetizations while t_1 and t_2 are the thickness of the RZ₁ and RZ₂ layers respectively. The magnetization of FM layer is denoted by \mathbf{m} .

polarization of the current in the respective RZ layers. Here, \mathbf{m} is the magnetization of the fixed FM layer of our system. Using Eqs. (2)-(4) in Eq. (1), we obtained six non linear coupled first order differential equations:

$$m'_{x1}[t] = \frac{\gamma}{1 + \alpha^2} \{ \alpha \mathcal{H}_{\text{eff}1} (m_{y1}^2 + m_{z1}^2) + \mathcal{H}_{\text{eff}2} (m_{z1} - \alpha m_{x1} m_{y1}) - \mathcal{H}_{\text{eff}3} (\alpha m_{x1} m_{z1} + m_{y1}) \} + \mathcal{P} \tau_1 [(\alpha (m_{x1}^2 + m_{y1}^2 + m_{z1}^2) \{ m_{y1} (m_{z2} - 1) - m_{y2} m_{z1} \} + m_{x1} \{ -m_{y1} m_{y2} - m_{z1} (m_{z2} - 1) \} + m_{x2} (m_{y1}^2 + m_{z1}^2))] \quad (6)$$

$$m'_{y1}[t] = \frac{\gamma}{1 + \alpha^2} \{ -\mathcal{H}_{\text{eff}1} (\alpha m_{x1} m_{y1} + m_{z1}) + \alpha \mathcal{H}_{\text{eff}2} (m_{x1}^2 + m_{z1}^2) + \mathcal{H}_{\text{eff}3} (m_{x1} - \alpha m_{y1} m_{z1}) \} + \mathcal{P} \tau_1 [(-\alpha (m_{x1}^2 + m_{y1}^2 + m_{z1}^2) \{ m_{x1} (m_{z2} - 1) - m_{x2} m_{z1} \} - m_{x1} m_{x2} m_{y1} + m_{x1}^2 m_{y2} - m_{y1} m_{z1} m_{z2} + m_{y1} m_{z1} + m_{y2} m_{z1}^2)] \quad (7)$$

$$m'_{z1}[t] = \frac{\gamma}{1 + \alpha^2} \{ \mathcal{H}_{\text{eff}1} (m_{y1} - \alpha m_{x1} m_{z1}) - \mathcal{H}_{\text{eff}2} (m_{x1} + \alpha m_{y1} m_{z1}) + \alpha \mathcal{H}_{\text{eff}3} (m_{x1}^2 + m_{y1}^2) \} + \mathcal{P} \tau_1 [\alpha (m_{x1}^2 + m_{y1}^2 + m_{z1}^2) (m_{x1} m_{y2} - m_{x2} m_{y1}) - m_{x1} m_{x2} m_{z1} + m_{x1}^2 m_{z2} - m_{x1}^2 - m_{y1} m_{y2} m_{z1} + m_{y1}^2 m_{z2} - m_{y1}^2] \quad (8)$$

$$m'_{x2}[t] = \frac{\gamma}{1 + \alpha^2} \{ \alpha \mathcal{H}_{\text{eff}4} (m_{y2}^2 + m_{z2}^2) + \mathcal{H}_{\text{eff}5} (m_{z2} - \alpha m_{x2} m_{y2}) - \mathcal{H}_{\text{eff}6} (\alpha m_{x2} m_{z2} + m_{y2}) \} + \mathcal{P} \tau_2 [(-m_{y2}^2 + m_{z2}^2) (m_{x1} - \alpha m_{y1} m_{z2} + \alpha m_{y2} m_{z1}) + \alpha m_{x2}^2 (m_{y1} m_{z2} - m_{y2} m_{z1}) + m_{x2} (m_{y1} m_{y2} + m_{z1} m_{z2})] \quad (9)$$

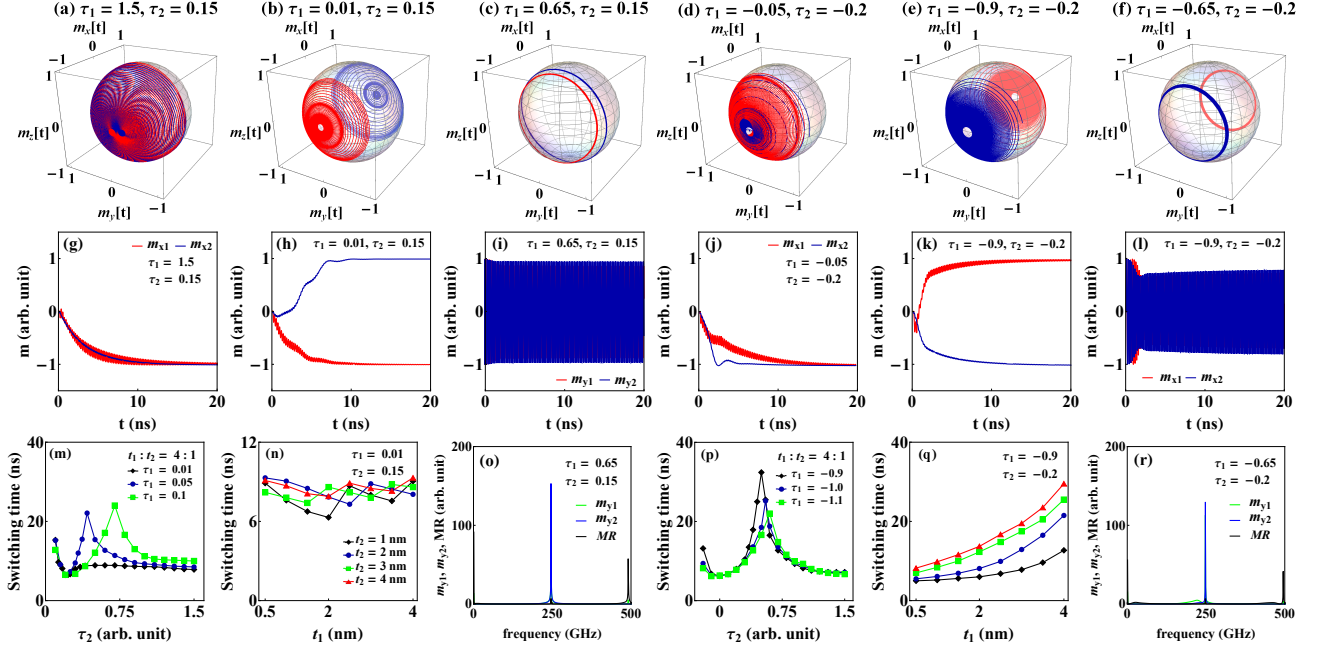


FIG. 2: (a) - (f) Oscillation trajectories of \mathbf{m}_1 (blue) and \mathbf{m}_2 (red) for different values of τ_1 and τ_2 considering $K_R = 0.1K_{DM}$. Plots (g) - (l) represent the time evolution of the magnetization component m_{x1} (red) and m_{x2} (blue). The variation of switching time with (τ_1, τ_2) and (t_1, t_2) are shown in plots (m), (p) and (n), (r) respectively. The Fourier transform of magnetization for (o) $(\tau_1, \tau_2) = (0.65, 0.15)$ and (r) $(\tau_1, \tau_2) = (-0.65, -0.2)$ respectively.

$$m'_{y2}[t] = \frac{\gamma}{1 + \alpha^2} \{ -\mathcal{H}_{\text{eff}4}(\alpha m_{x2} m_{y2} + m_{z2}) + \alpha \mathcal{H}_{\text{eff}5}(m_{x2}^2 + m_{z2}^2) + \mathcal{H}_{\text{eff}6}(m_{x2} - \alpha m_{y2} m_{z2}) \} + \mathcal{P}\tau_2 [\alpha(m_{x2}^2 + m_{y2}^2 + m_{z2}^2)(m_{x2} m_{z1} - m_{x1} m_{z2}) + m_{x1} m_{x2} m_{y2} - m_{x2}^2 m_{y1} - m_{y1} m_{z2}^2 + m_{y2} m_{z1} m_{z2}] \quad (10)$$

$$m'_{z2}[t] = \frac{\gamma}{1 + \alpha^2} \{ \mathcal{H}_{\text{eff}4}(m_{y2} - \alpha m_{x2} m_{z2}) - \mathcal{H}_{\text{eff}5}(m_{x2} + \alpha m_{y2} m_{z2}) + \alpha \mathcal{H}_{\text{eff}6}(m_{x2}^2 + m_{y2}^2) \} + \mathcal{P}\tau_2 [-\alpha(m_{x2}^2 + m_{y2}^2 + m_{z2}^2)(m_{x2} m_{y1} - m_{x1} m_{y2}) + m_{x1} m_{x2} m_{z2} - m_{x2}^2 m_{z1} + m_{y1} m_{y2} m_{z2} - m_{y2}^2 m_{z1}] \quad (11)$$

where,

$$\begin{aligned} \mathcal{H}_{\text{eff}1} &= -D_1 t_1 K_{DM} + h_0 - K_R m_{x2} - \alpha_R, \\ \mathcal{H}_{\text{eff}2} &= -D_1 t_1 K_{DM} + h_0 - K_R m_{y2} \\ \mathcal{H}_{\text{eff}3} &= K_{\text{an}} m_{z1} - H_{\text{ext}z} m_{z1} - D_1 t_1 K_{DM} + h_0 - K_R m_{z2} \\ \mathcal{H}_{\text{eff}4} &= -D_2 t_2 K_{DM} + h_0 - K_R m_{x1} - \alpha_R \\ \mathcal{H}_{\text{eff}5} &= -D_2 t_2 K_{DM} + h_0 - K_R m_{y1} \\ \mathcal{H}_{\text{eff}6} &= K_{\text{an}} m_{z2} - H_{\text{ext}z} m_{z2} - D_2 t_2 K_{DM} + h_0 - K_R m_{z1} \end{aligned}$$

III. RESULTS AND ANALYSIS

We investigate the magnetization dynamics and switching behaviour quantitatively by solving Eqs. (6)-(11) numerically.

We set the layer thickness, $t_1 : t_2 = 4 : 1$ and their respective polarizations as $\mathcal{P}_0 = \mathcal{P}_1 = 0.5$ for all our analysis [5]. This makes an asynchronism between m_{x1} and m_{x2} even in presence of RKKY. Moreover, other characteristics of magnetization dynamics like chaotic oscillations, magnetization switching etc can also be investigated under such condition. We also have explored different ratios of layer thickness and their impact on magnetization switching in our analysis. The RZ strength are set as $\alpha_R = 3 \times 10^{-10}$ eV.m and $h_0 = 0.7$ for all our analysis in Figs. 2 - 4. Furthermore, we set the DM coefficients $(D_1, D_2) = (-0.43, 0.43)$ are measured in mJ/m^2 for all our analysis [18]. The opposite sign of D_1 and D_2 are considered due to the opposite chirality of the induced DM interactions in $RZ_1|HM$ and $HM|RZ_2$ interfaces.

A. Interplay of RKKY with DM interaction

1. For systems with $RKKY < DM$ interaction

The magnetization oscillation and switching has been studied in Fig. 2 for $K_R = 0.1K_{DM}$ for different choices of (τ_1, τ_2) . We found that the system display magnetization switching in both positive and negative spin torque conditions, which are characterized by the positive and negative sign of τ_1 and τ_2 . Though the precession of the magnetic moments m_{x1} and m_{x2} are found to be identical for $(\tau_1, \tau_2) = (1.5, 0.15)$, but magnetization switching of m_{x2} is observed around $\tau_1 = 0.01$ as seen from Figs. 2(b) and (h). Moreover, the system is found to have stable magnetization oscillation in m_{x1} and m_{x2} for

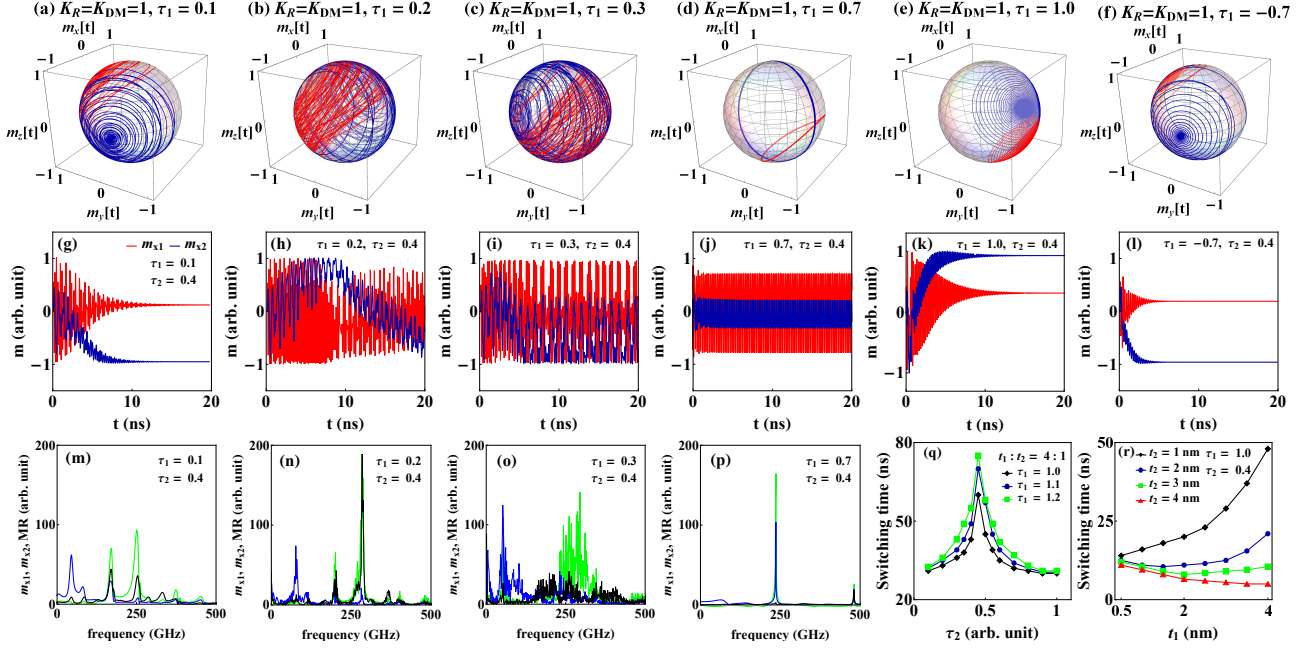


FIG. 3: (a) - (f) Oscillation trajectories of \mathbf{m}_1 (blue) and \mathbf{m}_2 (red) for different values of τ_1 considering $\tau_2 = 0.4$ and $K_R = K_{DM} = 1$. Plots (g) - (l) represent the time evolution of the magnetization component m_{x1} (red) and m_{x2} (blue). Plots (m) - (p) are the Fourier transform of the magnetization corresponding to the plots (g) - (j). The variation of switching time with (τ_1, τ_2) and (t_1, t_2) are shown in plots (q) and (r).

$\tau_1 = 0.65$, indicated by the Figs. 2(c) and (i). The sustained oscillations can be confirmed by a sharp peak around 250 GHz in the Fourier transform spectra of m_{x1} and m_{x1} . Thus for $\tau_1 = 0.65$ and $\tau_2 = 0.15$, the moments display a stable oscillation. It is to be noted that auto oscillation and the synchronization of the magnetizations can be measured by calculating GMR or TMR of the MTJ, where the resistance of the multi-layer is related to magnetization through \mathbf{m}_1 and \mathbf{m}_2 as [5]

$$\mathcal{R} = \frac{\mathcal{R}_{AP} + \mathcal{R}_P}{2} - \frac{\mathcal{R}_{AP} - \mathcal{R}_P}{2} \mathbf{m}_1 \cdot \mathbf{m}_2 \quad (12)$$

where, \mathcal{R}_P (\mathcal{R}_{AP}) is the resistance of the system corresponding to parallel (antiparallel) orientations of magnetization and the vector product $\mathbf{m}_1 \cdot \mathbf{m}_2$ can be termed as MR of the system. The synchronization of the magnetization \mathbf{m}_1 and \mathbf{m}_2 can be understood via two sharp MR peaks around 0 and 500 GHz as shown in Fig. 2(o). A similar characteristic of MR is also observed in Fig. 2(r) for negative biasing condition. The switching of m_{x1} for STT, $(\tau_1, \tau_2) = (-0.9, -0.2)$, is due to the opposite biasing of RZ_1 layer. However, the system can also behave like an oscillator even in negative biasing conditions for $\tau_1 = -0.65$ as seen from Figs. 2(f) and (l).

The variation of switching speed with τ_2 for both positive and negative values of τ_1 is studied in Figs. 2(m) and (p) respectively. The switching time (ST) can be numerically obtained by calculating the time corresponding to 97.5% of the saturation magnetization. It should be noted that for $\tau_1 = 0.01$, the ST gradually decreases for low values of τ_2 , but it remains constant in moderate and high τ_2 regions. Moreover, the switching speed decreases for $\tau_1 = 0.05$ and 0.1. In this condition, the maximum ST is found at $\tau_2 = 0.5$ and

0.7, respectively. An identical but opposite characteristic of magnetization switching is also observed for negative τ_1 values, as seen from Fig. 2(p). However, in this case, a delayed switching of m_{x1} is observed for lower values of τ_1 , which may be due to the opposite current biasing of the RZ_1 layer. Although the magnetization switching can occur for different (τ_1, τ_2) combinations as seen from Figs. 2(m) and 2(p), yet the interplay of STT with layer thickness and switching can be understood by exploring the variation of ST with layer thickness. Figs. 2(n) and 2(q) display the switching speed for $(\tau_1, \tau_2) = (0.01, 0.15)$ and $(\tau_1, \tau_2) = (-0.9, -0.2)$ respectively. For $(\tau_1, \tau_2) = (0.01, 0.15)$, the ST is found to be nearly same for all (t_1, t_2) . Nevertheless, the maximum switching speed is found for the thickness $t_1 = 2\text{nm}$ and $t_2 = 1\text{nm}$. The ST gradually increases with the increase in t_1 and t_2 for $(\tau_1, \tau_2) = (-0.9, -0.2)$ as seen from Fig. 2(q). Moreover, the switching speed slowed down with the increase in the thickness of the RZ_2 layer, as seen from Fig. 2(q).

2. For systems with $RKKY \sim DM$ interaction

The magnetization oscillations of the system are found to be very sensitive to τ_1 . As the RKKY interaction is of the order of DMI, as seen from Figs. 3(a) and (g). For $\tau_1 = 0.1$, the synchronization of \mathbf{m}_1 and \mathbf{m}_2 cease to exist. In this condition, \mathbf{m}_1 precesses about the z-axis while \mathbf{m}_2 about the x-axis. However, the oscillations are associated with multiple frequencies, as seen in Fig. 3(m). With a little increase in τ_1 to 0.2, the system executes non-linear oscillations as seen from Figs. 3(b) and (h). This nonlinearity is further enhanced

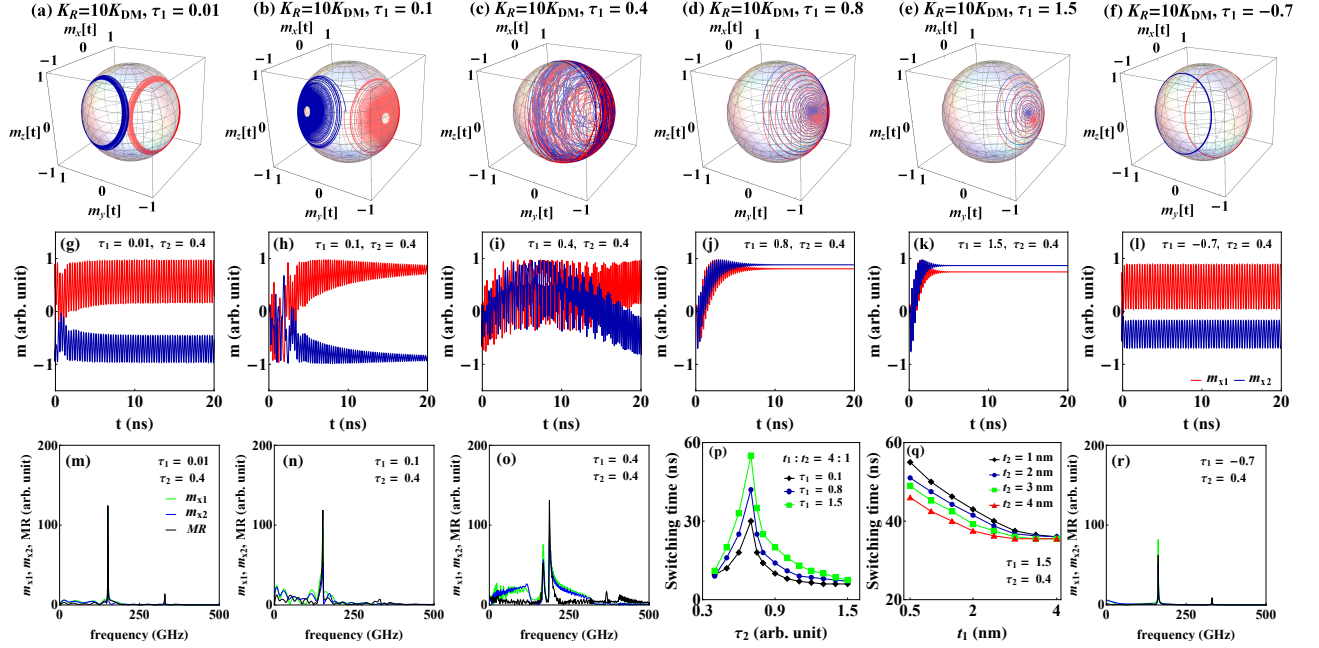


FIG. 4: (a) - (f) Oscillation trajectories of \mathbf{m}_1 (blue) and \mathbf{m}_2 (red), (g) - (l) the time evolution of the magnetization component m_{x1} (red) and m_{x2} (blue) for different values of τ_1 considering $\tau_2 = 0.4$ and $K_R = 10K_{DM}$. Plots (m) - (o) and (r) are the Fourier transform of the magnetization component, while plots (p) and (q) depicts the variation of switching time with τ_i and t_i respectively.

as τ_1 increases to 0.3 as indicated by Figs. 3(c) and (i). These non-linear oscillations can be characterized by the multiple frequencies in the Fourier spectra in 3(n) and (o). This may be due to the same order of RKKY and DM interaction which destabilizes the oscillations. However, sustained magnetization oscillations at about 250 GHz can be achieved with a further increase in τ_1 to 0.7 as suggested by Figs. 3(d) and (j). The switching characteristics can be studied by choosing $\tau_1 = 1.0$ and -0.7 as observed from Figs. 3(e), (f), (k) and (l). The ST vs τ_2 for different τ_1 has been studied in Fig. 3(q). It is seen that the rapid switching can be obtained by considering low values of τ_1 . It should be noted that the ST is identical with Fig. 2, but rapid switching is obtained for low values of τ_1 . Moreover, rapid switching is obtained for $t_1 = t_2 = 4$ nm. This indicates that by controlling the bias, current magnetization oscillations and switching can be achieved even when RKKY interaction is of the order DM interaction.

3. For systems with $RKKY > DM$ interaction

In Fig. 4, we study the magnetization dynamics for $K_R = 10K_{DM}$ with different choices of τ_1 considering $\tau_2 = 0.4$. The system executes sustained oscillations about the frequency 150 GHz for $\tau_1 = 0.01$ and -0.7 as seen from Figs. 4(a), (m), (f), and (r). However, for $\tau_1 = 0.01$, the system stabilizes after a short time, as indicated by Fig. 4(g). The switching characteristics are observed for $\tau_1 = 0.1$ and 0.8. However, it is to be noted that in this case, the magnetization reversal of \mathbf{m}_2 is observed as suggested by Figs. 4(b), (d), (h) and (j). With increase in τ_1 to 1.5, a rapid switching of \mathbf{m}_2 is seen in Fig. 4(e)

and (k). For moderate τ_1 , the system executes non-linear oscillations as seen from Fig. 4(c), (i) and (o). The dependence of ST with τ_1 and τ_2 is identical to that of Fig. 3. However, a gradual decrease in ST is observed with the rise in t_1 and t_2 as indicated by Fig. 4(p) and (q). Thus, the non-linear characteristics of the magnetization oscillations significantly decreases for $K_R > K_{DM}$ as compared to $K_R \sim K_{DM}$. Moreover, the frequency of oscillations also decreases in this scenario.

We observe that for $RKKY < DM$ interaction, the system behaves like a switcher for $0.01 < \tau_1 < 0.6$, oscillator for $0.6 < \tau_1 < 0.7$, while it remains unswitched for $0.7 < \tau_1 < 1$ in case of $\tau_2 > 0$. When $\tau_2 < 0$, the system remains unswitched for $-0.6 < \tau_1 < 0$ while behaves as an oscillator for $-0.65 < \tau_1 < -0.6$ and as a switcher for $-1 < \tau_1 < -0.65$ as seen from Fig. 2. For the systems with $RKKY \sim DM$ interaction, it shows unswitched characteristics for $-0.7 < \tau_1 < 0.2$, behaves as an oscillator for $0.6 < \tau_1 < 0.7$ and as a switcher for $0.7 < \tau_1 < 1$ considering $\tau_2 = 0.4$. Moreover, under this condition, the system display chaotic oscillations for $0.2 < \tau_1 < 0.6$ as seen from Fig. 3. Likewise, for the systems with $RKKY > DM$ interaction, oscillatory characteristics are seen for $-0.7 < \tau_1 < 0.1$, chaotic oscillations are found for $0.1 < \tau_1 < 0.4$ and the system remain unswitched for $0.4 < \tau_1 < 1.5$ considering $\tau_2 = 0.4$ as seen from Fig. 4.

B. Effect of RSOC

Even though magnetization dynamics in conventional ferromagnetic MTJs have been extensively explored, the impact

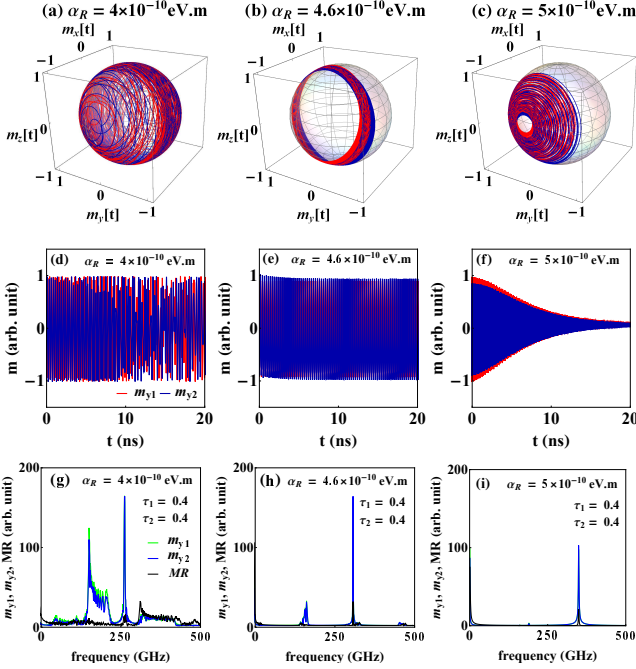


FIG. 5: Oscillation trajectories of \mathbf{m}_1 (blue) and \mathbf{m}_2 (red) for (a) $\alpha_R = 4 \times 10^{-10}$ eV.m, (b) $\alpha_R = 4.6 \times 10^{-10}$ eV.m and (c) $\alpha_R = 5 \times 10^{-10}$ eV.m considering $\tau_1 = \tau_2 = 0.4$ and $K_R = 10 K_{DM}$. Plots (d) - (f) are the time evolution of the magnetization component m_{y1} (red) and m_{y2} (blue) while plots (g) - (i) are the Fourier transform of the magnetization.

of SOC is yet to be understood. In general, SOC is responsible for splitting the spin-up and spin-down sub-bands. However, SOC can also significantly interplay with RKKY and DM interaction and, thus, affect the magnetization oscillations and reversal. Hence, in Fig. 5, we investigated the oscillations for different RSOC considering $h_0 = 0.7$, $\tau_1 = \tau_2 = 0.4$ and $K_R = 10 K_{DM}$. The system undergoes non-linear oscillations for $\alpha_R = 4 \times 10^{-10}$ eV.m as seen from Figs. 5(a) and (d). This can be characterized through the multiple oscillation frequencies from Fig. 5(g). The disappearance of non-linear oscillations for $\alpha_R = 4.6 \times 10^{-10}$ eV.m indicates stable magnetization oscillations as seen from Figs. 5(b) and (e). This can be confirmed from the sharp peak around 350 GHz in Fig. 5(h). With the further rise in $\alpha_R = 5 \times 10^{-10}$ eV.m, both \mathbf{m}_1 and \mathbf{m}_2 precess about the z-axis and decays slowly with an increase in time as seen from Figs. 5(c) and (f). The synchronized nature of these oscillations indicates the dominance of RKKY interaction in this system. So, RSOC can significantly impact RKKY and DM interactions, which indeed control the oscillations.

C. Effect of external magnetic field

To understand the interplay of an external magnetic field on RZ material, we study the magnetization dynamics and oscillations under low and moderate external magnetic field in Fig. 6, considering $\tau_2 = 0.4$, $\alpha_R = 3 \times 10^{-10}$ eV.m, $h_0 = 0.7$

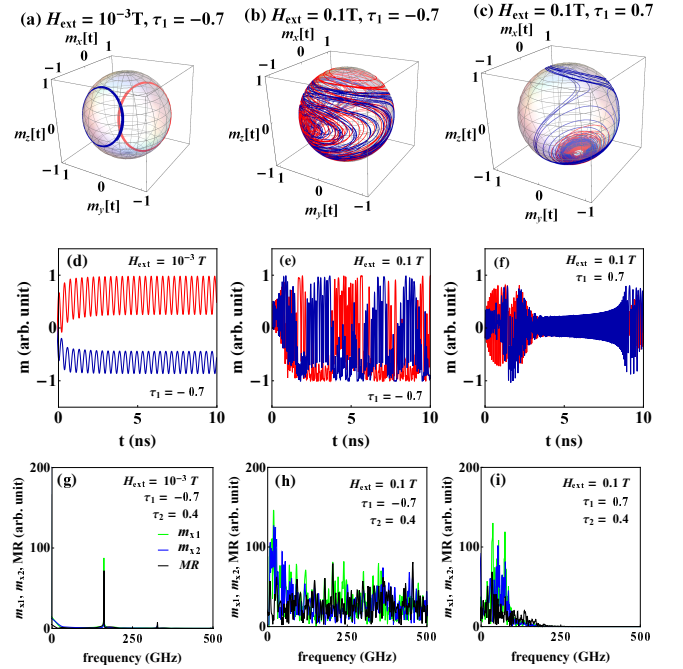


FIG. 6: Oscillation trajectories of \mathbf{m}_1 (blue) and \mathbf{m}_2 (red) for (a) $H_{ext} = 10^{-3}$ T, $\tau_1 = 0.7$ (b) $H_{ext} = 0.1$ T, $\tau_1 = 0.7$ and (c) $H_{ext} = 0.1$ T, $\tau_1 = -0.7$ considering $\tau_2 = 0.4$ and $K_R = 10 K_{DM}$. Plots (d) - (f) are the time evolution of the magnetization component m_{x1} (red) and m_{x2} (blue) while plots (g) - (i) are the Fourier transform of the magnetization.

and $K_R = 10 K_{DM}$. The system executes stable magnetization oscillations around frequency 180 GHz for $H_{ext} = 10^{-3}$ T as seen from Figs. 6(a), (d) and (g). This is because the impact of DM interaction and the external magnetic field is minimized for strong K_R . However, as the magnetic field is increased to 0.1 T, the synchronization of m_{x1} and m_{x2} due to K_R is broken. Thus, the system executes nonlinear oscillations as seen from Figs. 6(b) and (e). These nonlinear oscillations can be understood through the Fourier transform of the magnetization component in Fig. 6(h). Though the non-linear characteristics of the magnetization oscillations are found for $\tau_1 = -0.7$, the oscillations stabilize around the time range $\sim (3 - 8)$ ns for $\tau_1 = 0.7$ as seen from Fig. 6(f). As indicated by the Fourier spectra in Fig. 6(i), the magnetization display nonlinear oscillations under low low-frequency condition. This indicates that the oscillations not only depend upon the biasing current but can also be controlled through a suitable external magnetic field.

D. Interplay of RKKY, DM interaction with RSOC

Though the interplay of RKKY and DM interactions have been investigated for STT switching and oscillation in various previous works [18, 44–51] but the impact of RZ effect is yet to be understood. Fig. 7 depicts the magnetization dynamics in presence of STT for double-barrier RZ-MTJ under different h_0 and K_R and K_{DM} . It is observed that the magnetization os-

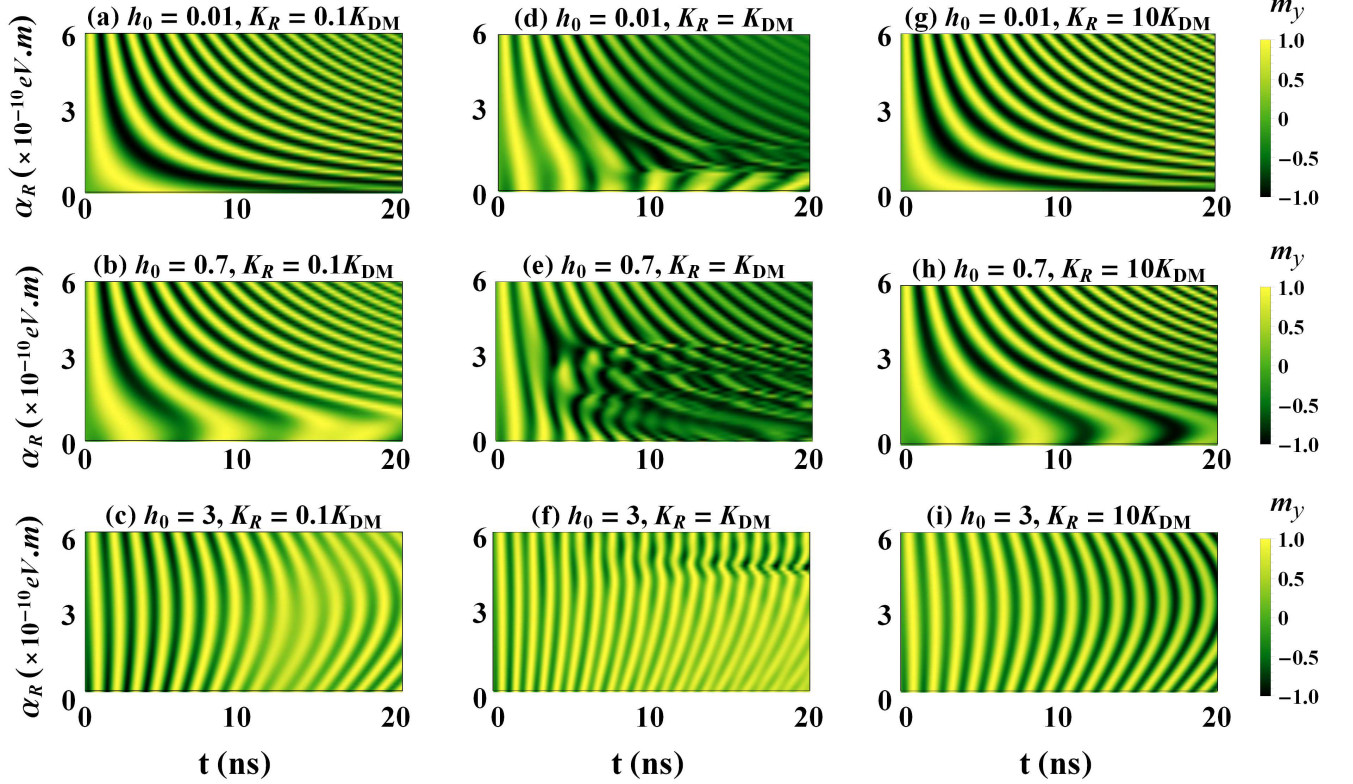


FIG. 7: Density plot of m_y with α_R and t for $h_0 = 0.01$ (top), $h_0 = 0.7$ (middle) and $h_0 = 0.01$ (bottom) with different choices of K_R and K_{DM} . The plots (a)-(c) in the left panel are for $K_R = 0.1K_{DM}$, (d)-(f) in the middle panel are for $K_R = K_{DM}$ while (g)-(i) in the right panel are for $K_R = 10K_{DM}$.

cillation under $K_R = 0.1 K_{DM}$ is quite similar with that of $K_R = 10 K_{DM}$ for corresponding choices of h_0 as seen from Figs. 7(a)-(c) and Figs. 7(g)-(i). We observe that with the increase in RSOC the magnetization oscillation also increases for low ($h_0 = 0.01$) and moderate ($h_0 = 0.7$) Zeeman strength. It is to be noted that the magnetization oscillation decays too rapidly as $\alpha_R \rightarrow 0$ for low values of h_0 while an oscillatory decay is observed at moderate h_0 . This is due to the reason that under low RZ energy, the Gilbert damping dominates the oscillations. However, the oscillations are still present in the system for suitable STT. The oscillations are too prominent under strong Zeeman condition even at low RSOC as seen from Fig. 7(c) as the required energy can be achieved from the exchange field. The oscillations slow down with time under moderate RSOC and high Zeeman energy. A non-linear characteristic of the magnetization orientation is observed as $K_R = K_{DM}$ as seen from the Figs. 7(d)-(f). This non-linear characteristics of m_y is too prominent for $h_0 = 0.7$ under moderate RSOC. This is due to the inconsistency of anisotropy of the corresponding magnetic layers at $K_R = K_{DM}$ [18]. However, this inconsistency can be eliminated by using Zeeman field strength $h_0 = 3$ as seen from Fig. 7(f) which can be used as a good oscillator.

IV. CONCLUSIONS

In summary, in this work the magnetization oscillations and switching have been investigated in the double-barrier RZ|HM|RZ MTJ in presence of Rashba-Zeeman, RKKY and DM interactions for different STTs. We observed that the system behaves as a good oscillator or a switcher when there exist a significant difference in the strength of RKKY and DM interaction. A nonlinear characteristics of the magnetization oscillation is observed as the order of RKKY interaction matches with the DM interaction. This double interface MTJ can also behave like a switcher for low and high STT when RKKY interaction is weaker than DM interaction. A similar characteristics can be seen for systems having strong RKKY interaction which signifies the interplay of RSOC on RKKY and DM interaction in RZ|HM|RZ MTJ. Though the magnetization oscillations are mostly nonlinear for systems having $RKKY \sim DMI$, the magnetization switching can still be tuned using suitable combinations of STT and RSOC. The oscillations are found to be sensitive to the coupling between external magnetic field and RZ interaction. The nonlinearity of oscillations can be significantly reduced by using suitable combination of external magnetic field and RZ interaction. It is noted that there exist a dependence of switching time on

layer thickness. The switching speed increases with thickness of the layers for systems having $RKKY \geq DM$ interactions while an opposite characteristics is seen for systems having $RKKY < DM$ interaction. Thus by choosing materials with

suitable RZ, RKKY and DM interactions, a double-barrier RZ|HM|RZ MTJ can be realized as a switcher or an oscillator using suitable STT.

-
- [1] J. C. Slonczewski, J. Magn. Magn. Mater, **159**, L1 (1996).
 - [2] J.C. Slonczewski, Phys. Rev. B **71**, 024411 (2005).
 - [3] L. Berger, Phys. Rev. B. **54**, 9353 (1996).
 - [4] N. Locatelli, V. Cros and J. Grollier, Nature Mat. **13**, 11 (2014).
 - [5] T. Taniguchi, J. Mag. Mag. Mater. **483**, 281-292 (2019).
 - [6] S. Acharjee and U. D. Goswami, J. Appl. Phys. **120**, 263902 (2016).
 - [7] J. Torrejon, et al. Nature **547**, 428–431 (2017).
 - [8] K. Kudo, T. Morie, Appl. Phys. Express, **10**, 043001 (2017).
 - [9] S. Tsunegi, et. al., Sci. Rep. **8**, 13475 (2018).
 - [10] M. Romera, et. al., Nature **230**, 563 (2018).
 - [11] Ø. Johansen and J. Linder, Sci. Rep. **6**, 33845 (2016).
 - [12] J. Grollier, D. Querlioz and M. D. Stiles, Spintronic Nanodevices for Bioinspired Computing, Proc. IEEE **104**, 2024 (2016).
 - [13] J. A. Katine, et. al. Phys. Rev. Lett. **84**, 3149 (2000).
 - [14] S.I. Kiselev, et. al., Nature **380**, 425 (2003).
 - [15] H. Kubota, et. al., Jpn. J. Appl. Phys. **44**, L1237 (2005).
 - [16] I.N. Krivorotov, et. al., Phys. Rev. B **76**, 024418 (2007).
 - [17] I.N. Krivorotov, Phys. Rev. B **77**, 054440 (2008).
 - [18] S. Li, et. al., Nanoscale Research Letters **14**, 315 (2019).
 - [19] J. Y. Choi, et. al., Sci Rep **8**(1), 2139 (2018).
 - [20] H. Sato, et. al., Appl Phys Lett **101**(2), 022414 (2012).
 - [21] S. Parkin, D. Mauri, Phys. Rev. B **44** 7131 (1991)
 - [22] I. Dzyaloshinsky, Phys Chem Solids **4**, 241 (1958).
 - [23] T. Moriya, Phys Rev **120**, 91 (1960).
 - [24] L. Tao and E. Y. Tsybal, npj Comput Mater **6**, 172 (2020).
 - [25] X. Xiao, et. al., J. App. Phys. **115**, 223709 (2014).
 - [26] P. Wójcik and J. Adamowski, Sci. Rep. **7**, 45346 (2017).
 - [27] S. Acharjee, et. al., arXiv:2209.11573, (2022).
 - [28] L. P. Gor'kov, E. I. Rashba, Phys. Rev. Lett. **87**, 037004 (2001).
 - [29] J. F. Liu, K.S. Chan and J. Wang, Nanotechnology **23** 095201 (2012).
 - [30] Q. Zhang, Z.J. Lin and K.S. Chan, Appl. Phys. Lett. **102**, 142407 (2013).
 - [31] L. Chico, A. Latge and L. Brey, Phys. Chem. Chem. Phys. **17**, 16469 (2015).
 - [32] S. Ganguly, S. Basu and S.K. Maiti, Europhys. Lett. **124** 57003 (2018).
 - [33] S. Ganguly, S. Basu, S.K. Maiti, Superlattices Microstruct. **120**, 650 (2018).
 - [34] A. A. Fouladi, Physica E, **102**, 117-122 (2018).
 - [35] Q. Zhang, J. Jiang and K.S.Chan, Physics Letters A **383** 2957–2962 (2019).
 - [36] J.-H. Liu, et. al., RSC Adv., **12**, 3386 (2022).
 - [37] S. LaShell, B. A. McDougall and E. Jensen, Phys. Rev. Lett. **77**, 3419 (1996).
 - [38] S. Acharjee and U. D. Goswami, Supercond. Sci. Technol. **32**, 085004 (2019).
 - [39] S. Acharjee and U. D. Goswami, J. Magn. Magn. Mater. **495**, 165844 (2020).
 - [40] S. Acharjee and U. D. Goswami, Physica E **135**, 114967 (2022).
 - [41] A. D. Caviglia, et al., Phys. Rev. Lett. **104**, 126803 (2010).
 - [42] K. Ishizaka, et. al., Nat. Mater. **10**, 521–526 (2011).
 - [43] Z. Duan, et. al., Nat. Commun **5**, 5616 (2014).
 - [44] S. Emori, et. al., Nat. Mater. **12**, 611 (2013).
 - [45] K. S. Ryu, et. al., Nat. Nanotechnol. **8** 527 (2013).
 - [46] S. Pizzini, et. al., Phys. Rev. Lett. **113**, 047203 (2014).
 - [47] M. Baumgartner, et. al., Nat. Nanotechnol. **12**, 980 (2017).
 - [48] A. Cao, et. al., Nanoscale **10**, 12062 (2018).
 - [49] O. Boulle, et. al., Phys. Rev. Lett. **111**, 217203 (2013).
 - [50] P. H. Jang, et. al., Appl. Phys. Lett. **107**, 202401 (2015).
 - [51] J. Sampaio, et. al., Appl. Phys. Lett. **108**, 112403 (2016).
 - [52] A. Chavent, et. al., ACS Appl. Electron. Mater. **3**, 2607-2613 (2021).

